

Enhanced proofreading governs CRISPR-Cas9 targeting accuracy

Janice S. Chen^{1*}, Yavuz S. Dagdas^{2*}, Benjamin P. Kleinstiver^{3,4*}, Moira M. Welch³, Lucas B. Harrington¹, Samuel H. Sternberg^{5†}, J. Keith Joung^{3,4}, Ahmet Yildiz^{1,6}, Jennifer A. Doudna^{1,5,7-8}

*These authors contributed equally to this work.

¹Department of Molecular and Cell Biology, University of California, Berkeley, California, 94720,

USA. ²Biophysics Graduate Group, University of California, Berkeley, California 94720, USA.

³Molecular Pathology Unit, Center for Cancer Research, and Center for Computational and

Integrative Biology, Massachusetts General Hospital, Charlestown, Massachusetts 02129, USA.

⁴Department of Pathology, Harvard Medical School, Boston, Massachusetts 02115, USA.

⁵Department of Chemistry, University of California, Berkeley, California 94720, USA.

⁶Department of Physics, University of California, Berkeley, California 94720, USA. ⁷Howard

Hughes Medical Institute, University of California, Berkeley, California 94720, USA. ⁸Physical

Biosciences Division, Lawrence Berkeley National Laboratory, Berkeley, California 94720, USA.

[†]Present address: Caribou Biosciences, Inc. Berkeley, California 94710, USA.

The RNA-guided CRISPR-Cas9 nuclease from *Streptococcus pyogenes* (SpCas9) has been widely repurposed for genome editing¹⁻⁴. High-fidelity (SpCas9-HF1) and enhanced specificity (eSpCas9(1.1)) variants exhibit substantially reduced off-target cleavage in human cells, but the mechanism of target discrimination and the potential to further improve fidelity were unknown⁵⁻⁹. Using single-molecule Förster resonance energy transfer (smFRET) experiments, we show that both SpCas9-HF1 and eSpCas9(1.1) are trapped in an inactive state¹⁰ when bound to mismatched targets. We find that a non-catalytic domain within Cas9, REC3, recognizes target mismatches and governs the HNH nuclease to regulate overall catalytic competence. Exploiting this observation, we identified residues within REC3 involved in mismatch sensing and designed a new hyper-accurate Cas9 variant (HypaCas9) that retains robust on-target activity in human cells. These results offer a more comprehensive model to rationalize and modify the balance between target recognition and nuclease activation for precision genome editing.

Efforts to minimize off-target cleavage by CRISPR-Cas9 have motivated the development of SpCas9-HF1 and eSpCas9(1.1) variants that contain amino acid substitutions predicted to weaken the energetics of target site recognition and cleavage^{8,9} (**Figure 1a**). Biochemically, we found that these Cas9 variants cleaved the on-target DNA with rates similar to that of wild-type (WT) SpCas9, whereas their cleavage activity was significantly reduced on substrates bearing mismatches (**Extended Data Figure 1a, 2a**). To test the hypothesis that SpCas9 with its single-guide RNA (sgRNA) might exhibit a greater affinity for its target than is required for effective recognition^{9,11}, we measured DNA binding affinity and cleavage of SpCas9-HF1 and eSpCas9(1.1) variants. Contrary to a potential hypothesis that mutating these charged residues to

alanine weakens target binding¹¹, the affinities of these variants for on-target and PAM-distal mismatched substrates were similar to WT SpCas9 (**Figure 1b, Extended Data Figure 1a, 2b**), indicating that cleavage specificity is improved through a mechanism distinct from a simple reduction of target binding affinity¹¹.

The HNH nuclease domain of SpCas9 undergoes a substantial conformational rearrangement upon target binding¹²⁻¹⁵, which activates the RuvC nuclease for concerted cleavage of both strands of the DNA^{12,16}. We have previously shown that the HNH domain stably docks in its active state with an on-target substrate but becomes loosely trapped in an catalytically-inactive conformational checkpoint when bound to mismatched targets¹⁰, suggesting that SpCas9-HF1 and eSpCas9(1.1) variants may employ a more stringent checkpoint to promote off-target discrimination. To test this possibility, we labeled catalytically active WT SpCas9 (SpCas9_{HNH}), SpCas9-HF1 (SpCas9-HF1_{HNH}) and eSpCas9(1.1) (eSpCas9(1.1)_{HNH}) with Cy3/Cy5 FRET pairs at positions S355C and S867C to measure HNH conformational states (**Figure 1c–f, Extended Data Figure 1c–e**)¹². Whereas SpCas9_{HNH} stably populated the active state with both on-target and mismatched substrates in steady-state smFRET histograms (**Figure 1d**), only ~32% of SpCas9-HF1_{HNH} molecules occupied the HNH active state ($E_{\text{FRET}} = 0.97$) with an on-target substrate, with the remaining ~68% trapped in the inactive intermediate state ($E_{\text{FRET}} = 0.45$) (**Figure 1e**). However, when SpCas9-HF1_{HNH} was bound to a substrate with just a single nucleotide mismatch at the PAM-distal end (20-20 bp mm), stable docking of the HNH nuclease was entirely ablated (**Figure 1e**). In addition, eSpCas9(1.1)_{HNH} and other high fidelity variants^{8,9} reduced the HNH active state in the presence of mismatches (**Figure 1f, Extended Data Figure 2c–d**). We therefore propose that high fidelity variants of Cas9 reduce off-target

cleavage by raising the threshold for HNH conformational activation when bound to DNA substrates.

Since the HNH domain does not directly contact nucleic acids at the PAM-distal end^{13,17-19}, it is likely that a separate domain of Cas9 senses mismatches to govern HNH domain mobility. Structural studies suggest that a domain within the Cas9 recognition (REC) lobe (REC3) interacts with the RNA/DNA heteroduplex and undergoes conformational changes upon target binding (**Extended Data Figure 3**)^{13,14,17-19}. Because the function of this non-catalytic domain was previously unknown, we labeled SpCas9 with Cy3/Cy5 dyes at positions S701C and S960C (SpCas9_{REC3}) and observed that the conformational states of REC3 become more heterogeneous as PAM-distal mismatches increase (**Extended Data Figure 4a-c**). To determine whether PAM-distal sensing precedes HNH activation, we deleted REC3 from WT Cas9 (SpCas9 Δ REC3) (**Figure 2a**). Deletion of REC3 decreased the cleavage rate by ~1000-fold compared to WT Cas9, despite retaining near-WT binding affinity with a perfect target (**Extended Data Figure 4d-f**). Unexpectedly, *in vitro* complementation of REC3 domain *in trans* rescued the on-target cleavage rate by ~100-fold in a concentration-dependent manner, but had no effect on cleavage with a PAM-distal mismatched target (**Figure 2b, Extended Data Figure 4e**). Furthermore, smFRET experiments revealed that the HNH domain in SpCas9 Δ REC3 (SpCas9 Δ REC3_{HNH}) occupied the active state only when REC3 was supplemented *in trans* (**Figure 2c-d, Extended Data Figure 4f**). We therefore propose that REC3 acts as an allosteric effector that recognizes RNA/DNA heteroduplex to allow for HNH nuclease activation.

We next considered allosteric interactions that could couple the discontinuous REC3 and HNH domains. Structural studies suggested that REC2 occludes the HNH domain from the

scissile phosphate in the sgRNA-bound state¹⁹, and undergoes a large outward rotation upon binding to double-stranded DNA (dsDNA)^{13,14} (**Figure 2e**). To test whether the REC2 domain regulates access of HNH to the target strand scissile phosphate, we labeled SpCas9 with Cy3/Cy5 dyes at positions E60C and D273C (SpCas9_{REC2}) in order to detect REC2 conformational changes (**Extended Data Figure 1b–c**). We observed reciprocal changes in bulk FRET values ($((\text{ratio})_A)^{20}$) between SpCas9_{HNH} and SpCas9_{REC2} across multiple DNA substrates (**Extended Data Figure 4g**), which suggest that the REC2 and HNH domains are tightly coupled to ensure catalytic competence. smFRET experiments further confirmed a large opening of REC2 during the transition from the sgRNA-bound state ($E_{\text{FRET}} = 0.96$) to the target-bound state ($E_{\text{FRET}} = 0.43$) (**Figure 2e–f**). In contrast to WT SpCas9_{REC2}, SpCas9-HF1_{REC2} occupies an intermediate state ($E_{\text{FRET}} = 0.63$) when bound to a target with just a single PAM-distal mismatch (**Figure 2f–g**). Together with the observation that the HNH domain of SpCas9-HF1 does not occupy the active state in the presence of PAM-distal mismatches, these experiments suggest that REC2 sterically occludes and traps the HNH nuclease domain in the conformational checkpoint when SpCas9 is bound to off-target substrates.

Next, we investigated if this conformational proofreading mechanism could be rationally exploited to design a suite of novel hyper-accurate Cas9 variants. We identified five clusters of residues containing conserved amino acids within 5 Å of the RNA/DNA interface, four of which are located within REC3 and one in the HNH-RuvC Linker 2 (L2) (**Figure 3a, Extended Data Figure 5**). Alone or in combination with Q926A, a substitution within L2 that confers specificity⁹, we generated alanine substitutions for each residue within five different clusters of amino acids (Clusters 1–5 ± Q926A) (**Figure 3a**). We tested whether these cluster mutations affected off-target discrimination and equilibrium binding *in vitro*, and found that Cluster 1 alone

and Cluster 2 + Q926A exhibited the greatest suppression of off-target cleavage while retaining target binding affinities comparable to WT (**Extended Data Figure 6**). We next screened all cluster variants in human cells using an enhanced GFP (*EGFP*) disruption assay⁵. On-target activity for Cluster 1 was comparable to that of SpCas9-HF1 or eSpCas9(1.1), whereas Cluster 2 variants displayed generally lower activity (**Figure 3b, Extended Data Figure 7a**). Furthermore, Cluster 1 retained high on-target activity (> 70% of WT) at 19/24 endogenous gene sites tested, compared to 18/24 for SpCas9-HF1 and 23/24 for eSpCas9(1.1) (**Figure 3c, Extended Data Figure 8a**).

We then focused on the specific contributions of mutations within Cluster 1 by restoring each individual mutated residue to its wild-type identity, along with the Q926A mutation, and testing the resulting variants for on-target editing efficiency in human cells. On-target activity was significantly compromised when N692A/Q695A/Q926A mutations occurred together, but restoring either N692 (Cluster 1 N692 + Q926A) or Q695 (Cluster 1 Q695 + Q926A) alone led to robust on-target efficiency comparable to Cluster 1, signifying differential contributions from these mutations to activity and specificity (**Extended Data Figure 7b-c, 8a-b**). Using sgRNAs with single mismatches against the endogenous human gene target *FANCF* site 1, we found that Cluster 1 exhibited even greater specificity than both SpCas9-HF1 and eSpCas9(1.1) in the middle and PAM proximal regions of the spacer, suggesting that mutating N692A and Q695A together may induce specificity in parts of the spacer sequence that were previously susceptible to off-target cleavage by high-fidelity Cas9 variants⁹ (**Figure 3d, Extended Data Figure 8c**). Additional single mismatch tolerance assays on *FANCF* sites 4 and 6 further corroborated the superior accuracy of Cluster 1 (N692A/M694A/Q695A/H698A, referred to as HypaCas9)

against mismatches at positions 1 through 18; however, single mismatches along *FANCF* site 2 were still tolerated across all SpCas9 variants tested (**Figure 3e, Extended Data Figure 8d, e**).

To biochemically validate cleavage specificity in the middle region of the spacer with HypaCas9, we measured cleavage rates against the *FANCF* site 1 sequence with or without internal mismatches at positions 10-12 of the spacer. Although HypaCas9 retained on-target activity comparable to WT and SpCas9-HF1 in human cells, its *in vitro* cleavage rate was slightly reduced for the one target site examined (**Figure 4a**). However, the cleavage rate with internally mismatched substrates was considerably slower compared to WT and SpCas9-HF1 (**Figure 4a**). This activity may be explained by the altered threshold of HNH domain activation; whereas stable HNH docking was observed by SpCas9_{HNH} and SpCas9-HF1_{HNH} with both the *FANCF* site 1 on-target and mismatched substrate at the 12th position, this HNH active state by HypaCas9 (HypaCas9_{HNH}) was diminished with the on-target. Nevertheless, HNH docking was nearly abolished when HypaCas9_{HNH} was bound to a substrate with a single mismatch (**Figure 4b**).

Our findings provide direct evidence to support previous speculation that Cas9 relies on PAM-distal protospacer sensing to enable accurate targeting^{21,22}. In particular, we define REC3 as an allosteric regulator of global Cas9 conformational changes to activate the nuclease domains, whose conformational threshold can be tuned for high-fidelity cleavage. Mutation of residues within REC3 that are involved in nucleic acid recognition, such as those mutated in HypaCas9 or SpCas9-HF1, prevents transitions by the REC lobe, which more stringently traps the HNH domain in the conformational checkpoint in the presence of mismatches (**Figure 4c, Extended Data Figure 9**). Curiously, nearly all of the amino acids within the cluster variants were strongly conserved (**Extended Data Figure 5**), suggesting that these residues may also be

involved in protospacer sensing and HNH nuclease activation across Cas9 orthologues.
 Furthermore, this observation may address how nature apparently has not selected for a highly
 precise Cas9 protein, whose native balance between mismatch tolerance and specificity may be
 optimized for host immunity. Our study therefore delineates a general strategy for improving
 Cas9 specificity by tuning conformational activation and offers innovative opportunities for
 rational design of hyper-accurate Cas9 variants that do not compromise efficiency.

METHODS

Protein purification and dye labeling. *S. pyogenes* Cas9 and truncation derivatives were cloned into a custom pET-based expression vector containing an N-terminal His₆-tag, maltose-binding protein (MBP) and TEV protease cleavage site. Point mutations were introduced by Gibson assembly or around-the-horn PCR and verified by DNA sequencing. Proteins were purified as described²³, with the following modifications: after Ni-NTA affinity purification and overnight TEV cleavage at 4°C, proteins were purified over an MBPTrap HP column connected to a HiTrap Heparin HP column for cation exchange chromatography. The final gel filtration step (Superdex 200) was carried out in elution buffer containing 20 mM Tris-HCl pH 7.5, 200 mM NaCl, 5% glycerol (v/v) and 1 mM TCEP. For FRET experiments, dye-labeled Cas9 samples were prepared as described¹². A list of all protein variants and truncations are listed in **Supplementary Table 1**.

Nucleic acid preparation. sgRNA templates were PCR amplified from a pUC19 vector containing a T7 promoter, 20 nt target sequence and optimized sgRNA scaffold. The amplified PCR product was extracted with phenol:chloroform:isoamylalcohol and served as the DNA template for sgRNA transcription reactions, which were performed as described²⁴. DNA oligonucleotides and 5'end biotinylated DNAs (Supplementary Table 2) were synthesized commercially (Integrated DNA Technologies), and DNA duplexes were prepared and purified by native PAGE as described²³.

DNA cleavage and binding assays. DNA duplex substrates were 5'-[³²P]-radiolabeled on both strands. For cleavage experiments, Cas9 and sgRNA were pre-incubated at room temperature for at least 10 min in 1X binding buffer (20 mM Tris-HCl pH 7.5, 100 mM KCl, 5 mM MgCl₂, 1 mM DTT, 5% glycerol, 50 µg ml⁻¹ heparin) before initiating the cleavage reaction by addition of DNA duplexes. For REC3 *in vitro* complementation experiments, SpCas9ΔREC3 and sgRNA were pre-incubated with 10-fold molar excess of REC3 for at least 10 minutes at room temperature before addition of radiolabeled substrate. DNA cleavage experiments were performed and analyzed as previously described¹². DNA binding assays were conducted in 1X binding buffer without MgCl₂ + 1 mM EDTA at room temperature for 2 hours. DNA-bound complexes were resolved on 8% native PAGE (0.5X TBE + 1 mM EDTA, without MgCl₂) at 4°C, as previously described¹⁰. Experiments were replicated at least three times, and presented gels are representative results.

Bulk FRET experiments. All bulk FRET assays were performed at room temperature in 1× binding buffer, containing 50 nM SpCas9_{HNH} (C80S/S355C/C574S/S867C labeled with Cy3/Cy5), SpCas9ΔREC3_{HNH}(M1–N497,GGG,V713–D1368 + C80S/S355C/C574S/S867C) or SpCas9_{REC2} (E60C/C80S/D273C/C574S labeled with Cy3/Cy5) with 200 nM sgRNA and DNA substrate where indicated. Fluorescence measurements were collected and analyzed as described¹². For REC3 *in vitro* complementation FRET experiments, SpCas9ΔREC3_{HNH} and sgRNA were pre-incubated with 10-fold molar excess of REC3 for at least 10 minutes at room temperature before measuring bulk fluorescence.

Sample preparation for smFRET assay. 99% PEG and 1% biotinylated-PEG coated quartz slides were received from MicroSurfaces, Inc. Sample preparation was performed as previously described¹⁰. To immobilize SpCas9 on its DNA substrate, 2.5nM biotinylated-DNA substrate introduced and incubated in sample chamber for 5 min. Excess DNA was washed with 1× binding buffer. SpCas9-sgRNA complexes were prepared by mixing 50 nM Cas9 and 50nM sgRNA in 1× binding buffer and incubated for 10 min at room temperature. SpCas9-sgRNA was diluted to 100 pM, introduced to sample chamber and incubated for 10 min. Before data acquisition, 20 μL imaging buffer (1 mg ml⁻¹ glucose oxidase, 0.04 mg ml⁻¹ catalase, 0.8% dextrose (w/v) and 2 mM Trolox in 1× binding buffer) was flown into chamber. The REC3 *in vitro* complementation assay was performed similar to steady-state FRET experiments: 2.5nM biotinylated-DNA substrate (on-target) was immobilized on surface, and excess DNA was washed with 1× binding buffer. SpCas9-sgRNA complexes were prepared by mixing 50 nM SpCas9ΔREC3 and 50nM sgRNA in 1× binding buffer and incubated for 10 min at room temperature. SpCas9-sgRNA was diluted to 100 pM, introduced to the sample chamber and incubated for 10 min. Before data acquisition, 20 μL imaging buffer was flown into chamber. After data acquisition, the sample chamber was washed with 1× binding buffer. 20 μL imaging buffer supplemented with 1μM REC3 was flown into sample chamber and incubated for 10min. After incubation, data for REC3 complementation was collected.

Microscopy and data analysis. A prism-type TIRF microscope was setup using a Nikon Ti-E Eclipse inverted fluorescent microscope equipped with a 60× 1.20 N.A. Plan Apo water objective and the perfect focusing system (Nikon). A 532-nm solid state laser (Coherent Compass) and a 633-nm HeNe laser (JDSU) were used for Cy3 and Cy5 excitation, respectively. Cy3 and Cy5

fluorescence were split into two channels using an Optosplit II image splitter (Cairn Instruments) and imaged separately on the same electron-multiplied charged-coupled device (EM-CCD) camera (512×512 pixels, Andor Ixon EM⁺). Effective pixel size of the camera was set to 267 nm after magnification. Movies for steady-state FRET measurements were acquired at 10 Hz under 0.3 kW cm⁻² 532-nm excitation. Data analysis was performed as described previously¹⁰. Briefly, two fluorescent channels were registered with each other using fiducial markers (20 nm diameter Nile Red Beads, Life Technologies) to determine the Cy3/Cy5 FRET pairs. Cy3/Cy5 pairs that photobleached in one step and showed anti-correlated signal changes were used to build histograms. FRET values were corrected for donor leakage and the histograms were normalized to determine the percentage of distinct FRET populations.

Human cell culture and transfection. Descriptions of nuclease and guide RNA plasmids used for human cell culture are available in **Supplementary Table 1 and 2**. Nuclease variants were generated by isothermal assembly into JDS246 (Addgene #43861)⁵, and guide RNAs were cloned into BsmBI digested BPK1520 (Addgene #65777)²⁵. Both U2OS cells (a gift from Toni Cathomen, Freiburg) and U2OS-EGFP cells (encoding a single integrated copy of a pCMV-EGFP-PEST cassette)²⁶ were cultured at 37 °C with 5% CO₂ in advanced DMEM containing 10% heat-inactivated fetal bovine serum, 2 mM GlutaMax, penicillin/streptomycin, and 400 µg ml⁻¹ Geneticin (for U2OS-EGFP cells only). Cell culture reagents were purchased from Thermo Fisher Scientific, cell line identities were validated by STR profiling (ATCC) and deep-sequencing, and cell culture supernatant was tested bi-weekly for mycoplasma. Transfections were performed using a Lonza 4-D Nucleofector with the SE Kit and the DN-100 program on ~200k cells with 750 ng of nuclease and 250 ng of guide RNA plasmids.

Human cell EGFP disruption assay. *EGFP* disruption experiments were performed as

previously described^{5,26}. Briefly, transfected cells were analyzed ~52 hours post-transfection for loss of EGFP fluorescence using a Fortessa flow cytometer (BD Biosciences). Background loss was determined by gating a negative control transfection (containing nuclease and empty guide RNA plasmid) at ~2.5% for all experiments.

T7 endonuclease I assay. Roughly 72 hours post-transfection, genomic DNA was extracted

from U2OS cells using the Agencourt DNAdvance Genomic DNA Isolation Kit (Beckman Coulter Genomics), and T7 endonuclease I assays were performed as previously described²⁶.

Briefly, 600–800 nt amplicons surrounding on-target sites were amplified from ~100 ng of genomic DNA using Phusion Hot-Start Flex DNA Polymerase (New England Biolabs) using the primers listed in Supplementary Table 2. PCR products were visualized (using a QIAxcel capillary electrophoresis instrument, Qiagen), and purified (Agencourt Ampure XP cleanup, Beckman Coulter Genomics). Denaturation and annealing of ~200 ng of the PCR product was followed by digestion with T7 endonuclease I (New England Biolabs). Digestion products were purified (Ampure) and quantified (QIAxcel) to approximate the mutagenesis frequencies induced by Cas9-sgRNA complexes.

REFERENCES

- 1 Doudna, J. A. & Charpentier, E. Genome editing. The new frontier of genome engineering with CRISPR-Cas9. *Science* **346**, 1258096, doi:10.1126/science.1258096 (2014).
- 2 Hsu, P. D., Lander, E. S. & Zhang, F. Development and applications of CRISPR-Cas9 for genome engineering. *Cell* **157**, 1262-1278, doi:10.1016/j.cell.2014.05.010 (2014).
- 3 Mali, P., Esvelt, K. M. & Church, G. M. Cas9 as a versatile tool for engineering biology. *Nat Methods* **10**, 957-963, doi:10.1038/nmeth.2649 (2013).
- 4 Barrangou, R. & Horvath, P. A decade of discovery: CRISPR functions and applications. *Nat Microbiol* **2**, 17092, doi:10.1038/nmicrobiol.2017.92 (2017).
- 5 Fu, Y. *et al.* High-frequency off-target mutagenesis induced by CRISPR-Cas nucleases in human cells. *Nat Biotechnol* **31**, 822-826, doi:10.1038/nbt.2623 (2013).
- 6 Tsai, S. Q. *et al.* GUIDE-seq enables genome-wide profiling of off-target cleavage by CRISPR-Cas nucleases. *Nat Biotechnol* **33**, 187-197, doi:10.1038/nbt.3117 (2015).
- 7 Tsai, S. Q. & Joung, J. K. Defining and improving the genome-wide specificities of CRISPR-Cas9 nucleases. *Nat Rev Genet* **17**, 300-312, doi:10.1038/nrg.2016.28 (2016).
- 8 Slaymaker, I. M. *et al.* Rationally engineered Cas9 nucleases with improved specificity. *Science* **351**, 84-88, doi:10.1126/science.aad5227 (2016).
- 9 Kleinstiver, B. P. *et al.* High-fidelity CRISPR-Cas9 nucleases with no detectable genome-wide off-target effects. *Nature* **529**, 490-495, doi:10.1038/nature16526 (2016).
- 10 Dagdas, Y. S., Chen, J. S., Sternberg, S. H., Doudna, J. A. & Yildiz, A. A Conformational Checkpoint Between DNA Binding And Cleavage By CRISPR-Cas9. *bioRxiv* (2017).

- 318 11 Bisaria, N., Jarmoskaite, I. & Herschlag, D. Lessons from Enzyme Kinetics Reveal
319 Specificity Principles for RNA-Guided Nucleases in RNA Interference and CRISPR-
320 Based Genome Editing. *Cell Syst* **4**, 21-29, doi:10.1016/j.cels.2016.12.010 (2017).
- 321 12 Sternberg, S. H., LaFrance, B., Kaplan, M. & Doudna, J. A. Conformational control of
322 DNA target cleavage by CRISPR-Cas9. *Nature* **527**, 110-113, doi:10.1038/nature15544
323 (2015).
- 324 13 Jiang, F. *et al.* Structures of a CRISPR-Cas9 R-loop complex primed for DNA cleavage.
325 *Science* **351**, 867-871, doi:10.1126/science.aad8282 (2016).
- 326 14 Palermo, G., Miao, Y., Walker, R. C., Jinek, M. & McCammon, J. A. Striking Plasticity
327 of CRISPR-Cas9 and Key Role of Non-target DNA, as Revealed by Molecular
328 Simulations. *ACS Cent Sci* **2**, 756-763, doi:10.1021/acscentsci.6b00218 (2016).
- 329 15 Palermo, G., Miao, Y., Walker, R. C., Jinek, M. & McCammon, J. A. CRISPR-Cas9
330 conformational activation as elucidated from enhanced molecular simulations. *Proc Natl*
331 *Acad Sci U S A*, doi:10.1073/pnas.1707645114 (2017).
- 332 16 Jinek, M. *et al.* A programmable dual-RNA-guided DNA endonuclease in adaptive
333 bacterial immunity. *Science* **337**, 816-821, doi:10.1126/science.1225829 (2012).
- 334 17 Nishimasu, H. *et al.* Crystal structure of Cas9 in complex with guide RNA and target
335 DNA. *Cell* **156**, 935-949, doi:10.1016/j.cell.2014.02.001 (2014).
- 336 18 Anders, C., Niewoehner, O., Duerst, A. & Jinek, M. Structural basis of PAM-dependent
337 target DNA recognition by the Cas9 endonuclease. *Nature* **513**, 569-573,
338 doi:10.1038/nature13579 (2014).

- 19 Jiang, F., Zhou, K., Ma, L., Gressel, S. & Doudna, J. A. STRUCTURAL BIOLOGY. A Cas9-guide RNA complex preorganized for target DNA recognition. *Science* **348**, 1477-1481, doi:10.1126/science.aab1452 (2015).
- 20 Majumdar, Z. K., Hickerson, R., Noller, H. F. & Clegg, R. M. Measurements of internal distance changes of the 30S ribosome using FRET with multiple donor-acceptor pairs: quantitative spectroscopic methods. *J Mol Biol* **351**, 1123-1145, doi:10.1016/j.jmb.2005.06.027 (2005).
- 21 Szczelkun, M. D. *et al.* Direct observation of R-loop formation by single RNA-guided Cas9 and Cascade effector complexes. *Proc Natl Acad Sci U S A* **111**, 9798-9803, doi:10.1073/pnas.1402597111 (2014).
- 22 Cencic, R. *et al.* Protospacer adjacent motif (PAM)-distal sequences engage CRISPR Cas9 DNA target cleavage. *PLoS One* **9**, e109213, doi:10.1371/journal.pone.0109213 (2014).
- 23 Jinek, M. *et al.* Structures of Cas9 endonucleases reveal RNA-mediated conformational activation. *Science* **343**, 1247997, doi:10.1126/science.1247997 (2014).
- 24 Wright, A. V. *et al.* Rational design of a split-Cas9 enzyme complex. *Proc Natl Acad Sci U S A* **112**, 2984-2989, doi:10.1073/pnas.1501698112 (2015).
- 25 Kleinstiver, B. P. *et al.* Engineered CRISPR-Cas9 nucleases with altered PAM specificities. *Nature* **523**, 481-485, doi:10.1038/nature14592 (2015).
- 26 Reyon, D. *et al.* FLASH assembly of TALENs for high-throughput genome editing. *Nat Biotechnol* **30**, 460-465, doi:10.1038/nbt.2170 (2012).

ACKNOWLEDGEMENTS

We thank Addison V. Wright, Stephen N. Floor, Joshua C. Cofsky, David Burstein, Christof Fellman, Benjamin L. Oakes and Orestes Mavrothalassitis for discussions and critical reading of the manuscript, and Michelle S. Prew for technical assistance. J.S.C. acknowledges support from the National Science Foundation Graduate Research Fellowship program, and B.P.K. from Banting (Natural Sciences and Engineering Research Council of Canada) and Charles A. King Trust Postdoctoral Fellowships. J.A.D. is an Investigator of the Howard Hughes Medical Institute. This work has been supported by NIH (GM094522 and GM118773 (A.Y.), R35 GM118158 (J.K.J.)), NSF (MCB-1617028 (A.Y.) and MCB-1244557 (J.A.D.)), and the Desmond and Ann Heathwood MGH Research Scholar Award (J.K.J.).

AUTHOR CONTRIBUTIONS

J.S.C., Y.S.D. and B.P.K. conceived of and designed experiments with input from L.B.H., S.H.S., J.K.J., A.Y. and J.A.D. J.S.C. performed protein expression, labeling and biochemical experiments. Y.S.D. performed single-molecule fluorescence assays and data analysis. B.P.K. and M.M.W. performed human cell-based experiments. J.S.C., Y.S.D., B.P.K., J.K.J., A.Y. and J.A.D. wrote the manuscript.

COMPETING FINANCIAL INTERESTS

J.K.J. has financial interests in Beacon Genomics, Beam Therapeutics, Editas Medicine, Pairwise Plants, Poseida Therapeutics, and Transposagen Biopharmaceuticals. J.K.J.'s interests were reviewed and are managed by Massachusetts General Hospital and Partners HealthCare in accordance with their conflict of interest policies. J.A.D. is a co-founder of Caribou Biosciences,

Editas Medicine, and Intellia Therapeutics; a scientific advisor to Caribou, Intellia, eFFECTOR
Therapeutics and Driver; and executive director of the Innovative Genomics Institute at UC
Berkeley and UCSF. S.H.S. is an employee of Caribou Biosciences, Inc. and an inventor on
patent applications related related to CRISPR-Cas systems and uses thereof. J.S.C, Y.S.D.,
B.P.K, L.B.H., S.H.S., A.Y., J.K.J. and J.A.D. are inventors on patents for CRISPR technologies.

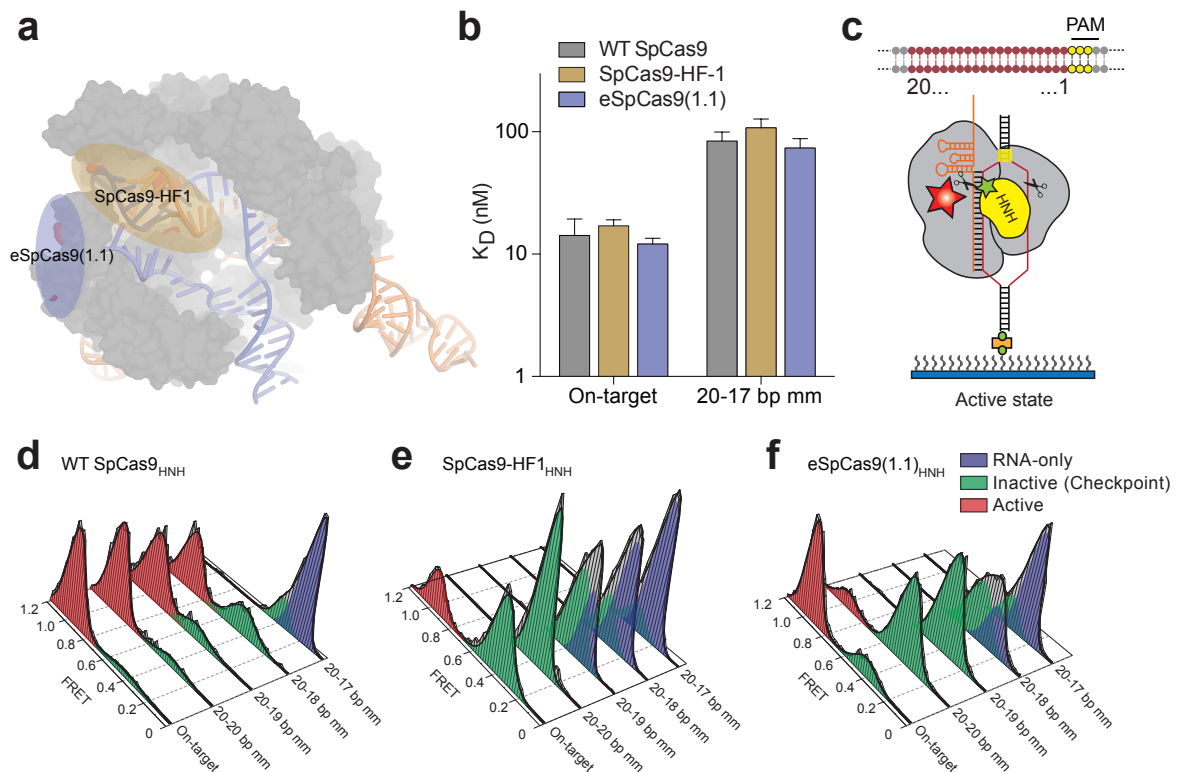


Figure 1 | High-fidelity Cas9 variants enhance cleavage specificity through HNH

conformational control. **a**, Locations of amino acid alterations present in existing high-fidelity SpCas9 variants mapped onto the dsDNA-bound SpCas9 crystal structure (5F9R), with the HNH domain omitted for clarity. **b**, Dissociation constants comparing WT SpCas9, SpCas9-HF1 and eSpCas9(1.1) with perfect and a 20-17 bp mismatched target. Error bars, s.d.; $n = 3$. **c**, Cartoon of DNA-immobilized SpCas9 complexes for smFRET experiments with DNA target numbering scheme. **d–f**, smFRET histograms measuring HNH conformational activation with **d**, WT SpCas9_{HNH}, **e**, SpCas9-HF1_{HNH} and **f**, eSpCas9(1.1)_{HNH} bound to perfect and PAM-distal mismatched targets. Black curves represent a fit to multiple Gaussian peaks.

FIGURE 2

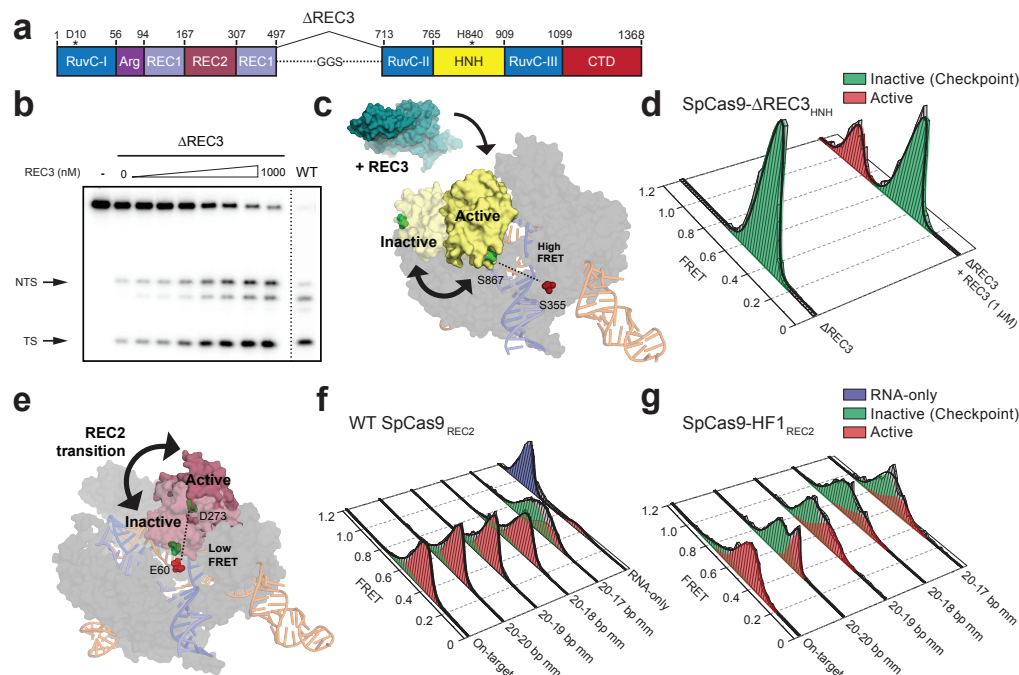


Figure 2 | The alpha-helical lobe regulates HNH domain activation. **a**, Domain organization of SpCas9ΔREC3. **b**, Perfect target DNA cleavage assay using SpCas9ΔREC3 with increasing concentrations of REC3 domain supplied in *trans*, resolved by denaturing PAGE. **c**, Schematic of SpCas9ΔREC3_{HNH} with FRET dyes at positions S355C and S867C, with the REC3 domain added *in trans*. Inactive to active structures represent HNH in the sgRNA-bound (PDB ID: 4ZT0) to dsDNA-bound (PDB ID: 5F9R) forms, respectively. **d**, smFRET histograms measuring HNH conformational states with SpCas9ΔREC3_{HNH} in the absence and presence of the REC3 domain. **e**, Schematic of SpCas9_{REC2} with FRET dyes at positions E60C and D273C, with HNH domain omitted for clarity. Inactive to active structures represent REC2 in the sgRNA-bound (PDB ID: 4ZT0) to dsDNA-bound (PDB ID: 5F9R) forms, respectively. **f-g**, smFRET histograms measuring REC2 conformational states with **f**, WT SpCas9_{REC2} and **g**, SpCas9-HF1_{REC2} bound to perfect and PAM-distal mismatched targets. For panels **d**, **f** and **g**, black curves represent a fit to multiple Gaussian peaks.

FIGURE 3

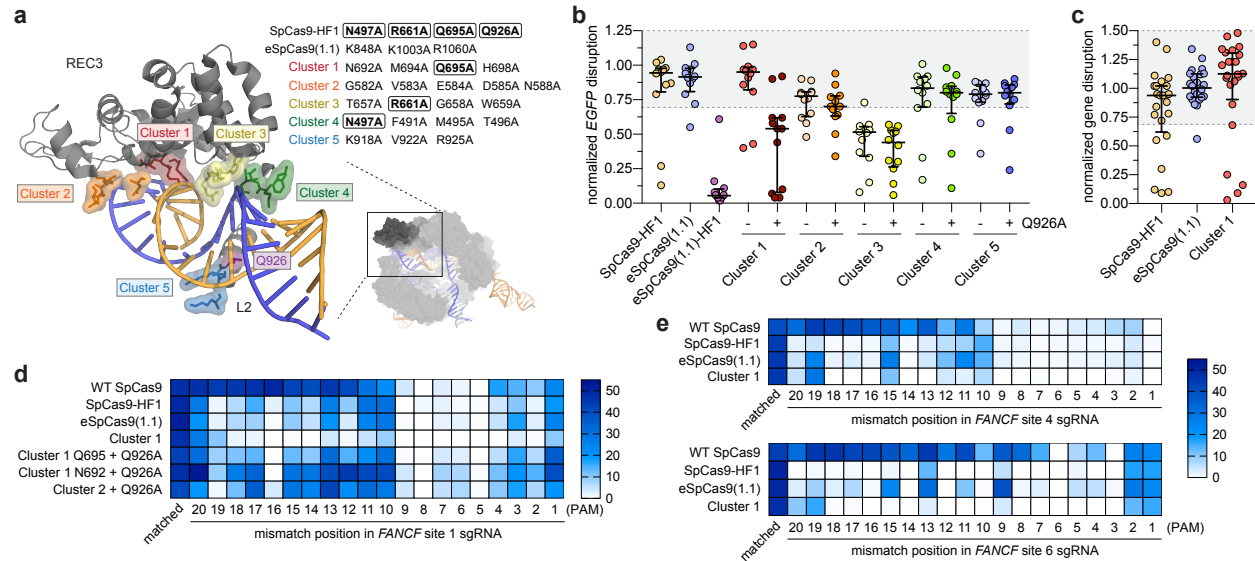


Figure 3 | Targeted mutagenesis within the REC3 domain reveals a SpCas9 variant with hyper-accurate behavior in human cells. **a**, Zoomed image of the REC3 domain and Linker 2 (L2) with Cluster variants indicated. Boxed residues indicate amino acids also present in SpCas9-HF1. **b**, WT-normalized activity of SpCas9-HF1, eSpCas9(1.1) and Cluster variants, using sgRNAs targeting 12 different sites within *EGFP*. **c**, WT-normalized endogenous gene disruption activity measured by T7 endonuclease 1 (T7E1) assay across 24 sites. **d**, Activities of WT and high-fidelity Cas9 variants when programmed with singly mismatched sgRNAs against *FANCF* site 1 as measured by T7E1 assay. **e**, Activities of WT SpCas9, SpCas9-HF1, eSpCas9(1.1) and Cluster 1 when programmed with singly mismatched sgRNAs against *FANCF* site 4 and *FANCF* site 6. For panels **b** and **c**, error bars represent median and interquartile ranges, and $n \geq 3$; the interval with $> 70\%$ of wild-type activity is highlighted in light grey.

FIGURE 4

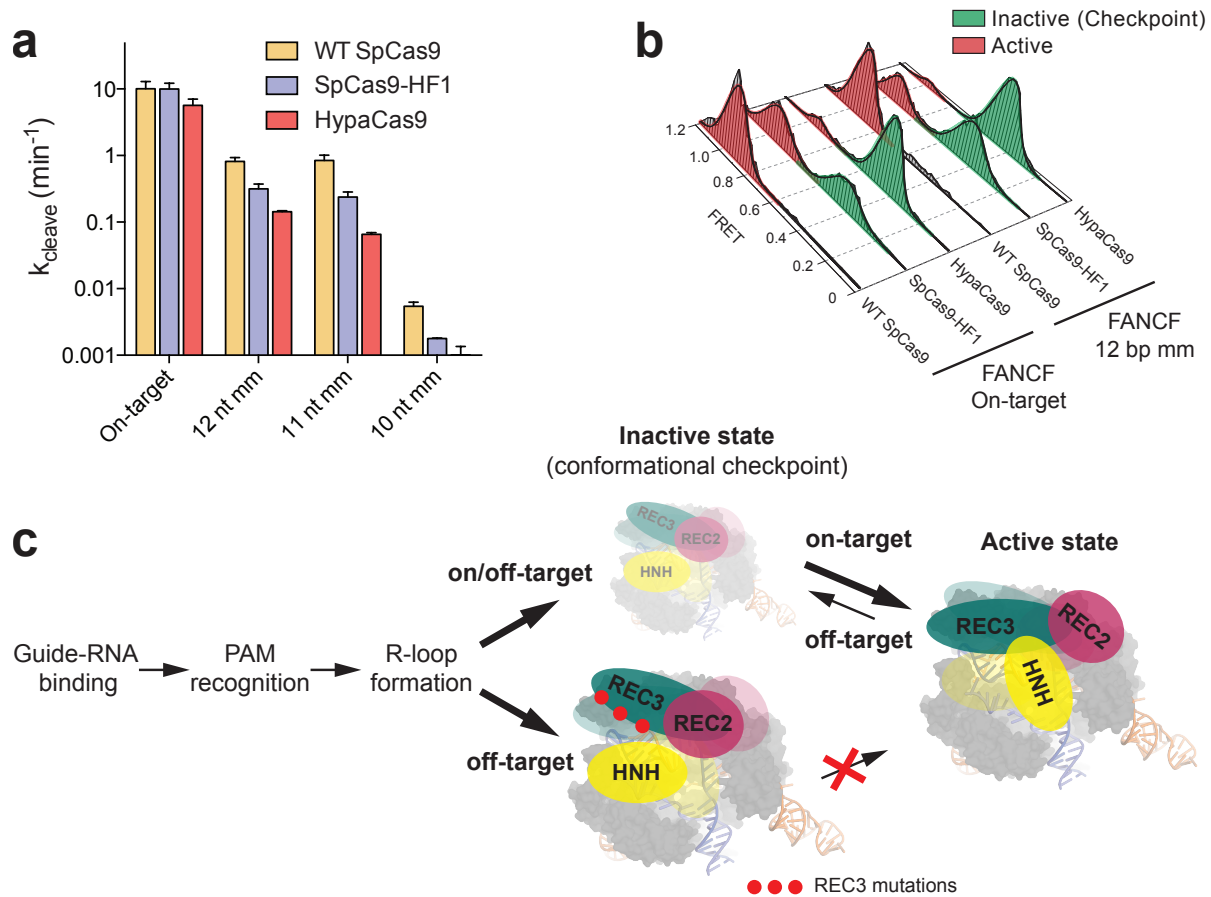


Figure 4 | Mutating residues involved in proofreading increases the threshold for conformational activation to ensure targeting accuracy. a, DNA cleavage kinetics of SpCas9 variants with the *FANCF* site 1 on-target and internally mismatched substrates. Error bars, s.d.; $n = 3$. **b**, smFRET histograms measuring HNH conformational states for indicated SpCas9 variants with a *FANCF* site 1 on-target and mismatched substrate at the 12th position; black curves represent a fit to multiple Gaussian peaks. **c**, Model for alpha-helical lobe sensing and regulation of the RNA/DNA heteroduplex for HNH activation and cleavage.